International Journal of Modern Manufacturing Technologies
ISSN 2067–3604, Vol. VIII, No. 1 / 2016

# INTERNAL FRICTION EVALUATION IN MECHANICALLY ALLOYED-POWDER METALLURGY Fe-Mn-Si-Cr-Ni SHAPE MEMORY ALLOYS

**E. Mihalache[1], B. Pricop[1]*, N.-M. Lohan[1], M.-G. Suru[1], B. Ozkal[2], L.-G. Bujoreanu[1]**

[1] Faculty of Materials Science and Engineering, "Gheorghe Asachi" Technical University of Iasi-Romania, Blvd. Dimitrie Mangeron 67, 700050 Iași, Romania;
[2] Particulate Materials Laboratory, Metallurgical and Materials Engineering Department, Istanbul Technical University, 34469 Maslak, Istanbul, Turkey

Corresponding author: Leandru-Gheorghe Bujoreanu, lgbujor@tuiasi.ro

***Abstract:*** Fe-Mn-Si-Cr-Ni Shape Memory Alloys (SMAs) were manufactured from as blended powders (0_MA) and powders with 10 % and 20 % particles obtained after mechanical alloying (10_MA and 20_MA, respectively). The specimens were hot rolled, to increase the compactness degree, and solution treated to five different temperatures, being finally water quenched, to retain martensitic phases. The present study aims to emphasize the influence of: (i) MA fraction and (ii) solution treatment temperature on the storage modulus and internal friction as a function of temperature and amplitude, under constant frequency. For this purpose, Dynamic-Mechanical Analyses (DMA) were conducted both by temperatures scans and by strain sweeps. During temperature scans, the strain was kept constant. Strain sweeps were performed, at 3 temperatures ($T_1$=RT, $A_s<T_2<A_{50}$ and $T_3>A_{50}$, where $A_s$ and $A_{50}$ are the critical temperatures for the start and middle of reverse transformation of martensite to austenite). A modulus increase and double internal friction maxima were observed on heating and maximum internal friction was measured at $T_2$.
***Key words:*** shape memory alloys, dynamic-mechanical analysis, mechanical alloying, heat treatment, martensite.

## 1. INTRODUCTION

Vibrational damping is caused by energy dissipation during mechanical vibrations/ deformations of an elastic body, associated with the irreversible conversion to thermal energy or to sound (Banks and Pinter, 2001). This irreversible conversion of mechanical to thermal energy is generally termed internal friction (IF) being estimated by a quality factor Q representing its reciprocal value:

$$Q^{-1} = IF \quad (1)$$

The global internal friction ($Q^{-1}_{tot}$) spectrum has various forms as a function of the thermomechanical history of the material and the relative values of interface mobility (De Jongue *et al.*, 1976). Its value represents the sum of three contributions: (i) $Q^{-1}_{Tr}$ - transitory term, proportional to the volume fraction transformed per unit of time, existing only during temperature variation (most important part within the frequency range around 1 Hz); (ii) $Q^{-1}_{PT}$ - phase transition term associated with the phase transition itself, at constant temperature, and related to the reversible displacement of interfaces; and (iii) $Q^{-1}_{Int}$ - the intrinsic term that considers damping generated in the coexisting phases (Van Humbeeck *et al.*, 1995). Determining the values of each term, under specific conditions, requires their separation from the internal friction spectrum (Perez-Saez *et al.*, 1998).
In literature, besides internal friction, $Q^{-1}$ is designated under various names, such as: *loss factor* (Van Humbeeck *et al.*, 1995), *tan φ* or *tan delta (δ)* (Van Humbeeck, 2001). The latter originates from the ratio between the imaginary and the real parts of the complex compliance of a material system, S = S' +i·S" (Magalas, 2003):

$$\tan \delta = S"/ S' \quad (2)$$

The relationship between internal friction and damping is expressed by means of the Specific Damping Capacity (SDC), representing the percentage ratio between dissipated (ΔW) and total consumed energy (W) during one loading-unloading mechanical cycle, and has the form (Montecinos, (2015):

$$SDC = \Delta W/ W = 2\pi \cdot Q^{-1} \quad (3)$$

There is no unique damping capacity for one material, since it depends on both external (temperature, time, frequency, amplitude) and internal parameters (material state, grain size, defect structure, inter-phase mobility). However, under standard conditions, metallic materials have been divided into low (SDC < 1 %); medium (SCD = 1-10 %) and high damping materials (SDC > 10 %). The last category was subdivided into 4 types: (i) natural composites; (ii) ferromagnetic; (iii) dislocation and

(iv) twin or inter-phase boundary (Baik, S. H., 2006).
In twin or inter-phase boundary type high-damping materials, internal friction is caused by the hysteretic movement of interfaces during the stress induced transformations or the crystalline reorientations of metallographic phase variants (Bidaux *et al.*, 1989). In the specific case of metallic materials experiencing martensite transformation, one of the controlling factors of interface movement is the dissipation of frictional energy due to the interactions with crystals defects (Stoiber *et al.*, 1994) such as precipitates (Baik *et al.*, 1997), dislocations (Granato and Lucke, 1956), stacking faults (Jee *et al.*, 1994) or grain boundaries (Jee *et al.*, 1985).
Aiming to systematically evaluate the mechanism of IF, accompanying the reverse martensitic transformation from ε hexagonal close-packed (hcp) martensite to γ face cantered cubic (fcc) austenite in an Fe-Mn-Si based shape memory alloy (SMA), a logarithmic decrement maximum (tan δ peak) of almost 0.03, was determined which was associated with the motion of Schockley partial dislocations (Sato *et al.*, 1988). Later, aiming to demonstrate the elevated damping capacity of non-thermoelastic alloys, a binary Fe-17 wt. %Mn alloy was developed, experiencing a SDC = 0.28 (Choi *et al.*, 1992) which, by means of equation (3), gives an IF value of $Q^{-1} \approx 0.044$. This performance was further increased to SDC ≈ 0.36 ($Q^{-1} \approx 0.057$) as an effect of cold working (Baik *et al.*, 1995), being associated with the maximization of γ/ ε interface surface area (Lee *et al.*, 1997). In addition, at high damping materials of interphase boundary type, evidence was brought that IF strongly depends on interface mobility (Jee *et al.*, 1997). Considering the similarities between the mechanism of internal friction and that of shape memory effect (SME), which both rely on the reverse movement of γ/ ε interface (Kajiwara, 1999), intensive studies were carried out on the relationship between IF behaviour and the stress-induced formation of ε-hcp martensite from γ-fcc austenite, in Fe-Mn based SMAs (De, *et al.*, 2002). With the development of Fe-Mn-Si based SMAs, by addition of Cr and Ni, it has been observed that the necessary thickness reduction, to about 1 nm, of ε-martensite plates, caused by training (Kajiwara *et al.*, 2001) or by the formation of nano-precipitates, such as NbC (Sawaguchi *et al.*, 2006a), is accompanied by a much more prominent enhancement of shape recovery than of damping capacity (Sawaguchi. *et al.*, 2006b).
The elevated IF values observed at Fe-Mn-Si-based SMAs have recommended them as base material for antiseismic dampers (Sawaguchi *et al.*, 2006c) due to the reversible stress-induced formation of ε-hcp martensite or of mechanical γ-fcc twins (Sawaguchi *et al.*, 2007).
However, there are still very large differences between the IF values reported at binary Fe-17 mass. % Mn (tan Φ ≈ 0.083) (Sawaguchi *et al.*, 2008) and those currently measured at classical metallurgy-processed SMAs, such as Fe-Mn-Si-Cr Ni (tan Φ ≈ 0.033) (Bujoreanu. *et al.*, 2009) or Fe-Mn-Si-C (tan Φ ≈ 0.042) (Min *et al.*, 2013). On the other hand, the presence of porosity in SMAs was reported as a source of damping enhancement (Kothalkar *et al.*, 2014), associated with marked increases of IF peak intensity, of the reverse martensitic transformation, in porous materials (Wang *et al.* 2014).
For this reason, the present paper focuses on the evolution of IF behaviour, evaluated by Dynamic-Mechanical Analysis (DMA), in the case of powder metallurgy (PM) Fe-Mn-Si-Cr-Ni SMAs, while considering the possibility to improve their shape memory characteristics via heat treatment and mechanical alloying (MA) (Söyler *et al.* 2014).

## 2. EXPERIMENTAL PROCEDURE

Three groups of parallelepipedal specimens, with nominal chemical composition 66Fe-14Mn-6Si-9Cr-5Ni (mass %), were pressed and sintered under argon atmosphere. The first group, 0_MA, was obtained from as-blended elemental powders (Pricop *et al.* 2012). The second (10_MA) and third (20_MA) groups comprised 10 vol. % and 20 vol. % fractions of mechanically alloyed (MA) powders, respectively, obtained after high energy ball milling under argon atmosphere (Söyler *et al.* 2011) for the duration of 4 hours, which enabled optimal densification of compacted samples (Söyler *et al.* 2010). In order to further increase specimens' compactness, six consecutive hot rolling passes were performed at 1373 K, without allowing the billets to cool down to room temperature (RT), until reaching a thickness of 1 mm *(*Pricop *et al.*, 2014*)*. After hot rolling, specimens' densities were measured with an electronic scales equipped with a special kit for the determination of apparent density: 0_MA – 6.206 g/ $cm^3$; 10_MA – 6.865 g/ $cm^3$ and 20_MA - 7.028 g/ $cm^3$. The density of the compact Fe-Mn-Si-Cr-Ni SMA would be approx. 7.464 g/$cm^3$. Therefore the alloys under study have the following degrees of porosity: 16.85 % for 0_MA; 8.03 % for 10_MA and 5.94 % for 20_MA. After machining and spark erosion cutting, hot-rolled lamellar specimens were solution treated at five different temperatures between 973, 1073, …, 1373K/ held 300 s and water quenched (Spiridon *et al.*, 2013). Since at least 4 specimens were prepared from each of the 15 differently processed sets, it follows that more than 60 specimens were subjected to two kinds of experiments: (i) temperature scans and (ii) strain sweeps. These experiments were performed by means of a dynamic mechanical analyser (DMA) type DMA 242 Artemis NETZSCH, with force resolution of

0.0005 N, amplitude range: ± 0.1 up to 240 μm and amplitude resolution: 0.0005 μm. A specimen holder type three-point bending was used and a maximum static pre-loading force of 12 N. The specimens were tested at a constant frequency of 1 Hz, under Ar protective atmosphere, using liquid nitrogen cooling.

### 2.1 Temperature scans

The first type of DMA experiments comprised heating-cooling cycles (temperature scans), from RT to 673 K and back to RT, performed, with a temperature variation rate of 5 K/ min and amplitude of 20 μm (strain amplitude of 0.02). The results were recorded as DMA thermograms illustrating the variation of storage modulus (E') and internal friction (tan δ) as a function of temperature. One typical variation of E' and tan δ during heating, at binary Fe-Mn, is shown in Fig. 1 (Sawaguchi *et al.*, 2008a).

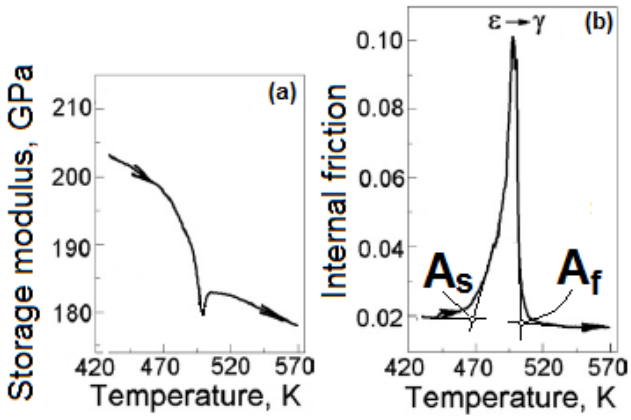


Fig.1 Typical schematic DMA thermogram recorded during the heating of a Fe-Mn alloy: (a) storage modulus variation with temperature; (b) internal friction variation with temperature.

Besides $A_s$ and $A_f$ critical temperatures, determined by the tangent method (Lohan *et al.*, 2011), there is a transformation peak at the critical temperature $A_{50}$, where 50 % martensite transformed to austenite. It corresponds to the middle of martensite reversion and also to the internal friction peak.

### 2.2 Strain sweeps

The second type of DMA experiments were isothermal strain sweeps, performed at three different temperatures: (i) $T_1$ = RT, (ii) $A_s < T_2 < A_{50}$ and (iii) $T_3 > A_{50}$. Within each strain sweep three bending cycles were applied with amplitude varying in 20 equal steps between 0.1 and 200 μm, (strain amplitudes between 0.0001 and 0.2).

Considering that internal friction is highly sensitive to constitutional structures (Chou *et al.*, 2000), XRD patterns were recorded on the significance region 2θ = 30-100°, using an Expert PRO MPD diffractometer with Cu $K_\alpha$ radiation. The corresponding crystallographic databases 00-034-0396, 01-071-8285 and 01-071-8288, were used for the identification of the constitutive metallographic phases α'-martensite (body centred cubic-bcc), ε-martensite (hcp) and γ-austenite (fcc), respectively.

## 3. RESULTS AND DISCUSSION

### 3.1 DMA during temperature scans

The first DMA thermograms were recorded during one heating-cooling cycle of specimen 0_MA_700 (heat treated at 973 K). Fig. 2 illustrates the typical variations with temperature of storage modulus (E') and internal friction (tanδ), smoothened with PROTEUS software, which controls the functioning of DMA device.

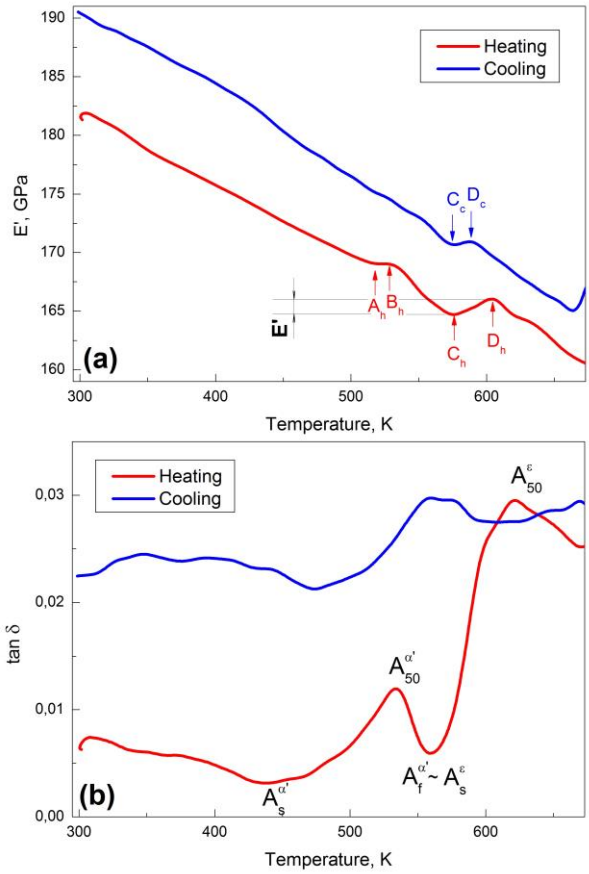


Fig. 2 DMA thermograms recorded in a heating-cooling cycle of 0_MA_700 specimen: (a) variation of storage modulus with temperature; (b) variation of internal friction with temperature

At Fe-Mn-Si based SMAs, it is well known that the presence of internal friction peaks is accompanied by modulus defect (Gavrijuk *et al.*, 1998) such as the local drop in storage modulus, observed in Fig. 1(a), during heating, in the proximity of $A_f$ temperature. Considering that the modulus of ε phase is higher than that of γ phase, a so-called "modulus softening" was associated with ε → γ transformation during heating (Wan *et al.*, 2006). Between the temperatures

of the starting and ending points of modulus softening (decrease) on heating and that corresponding to the beginning and ending of internal friction (tan δ) peaks, respectively, there is always a discrepancy (Wu *et al.*, 2000).

For this reason, there is a slight shift in the temperature range of modulus decrease, in Fig. 2(a) and that of the internal friction peak, in Fig. 2(b). In Fig. 2(a) each stage of modulus softening is preceded by a hardening stage, as follows: $A_hB_h$ –hardening and $B_hC_h$ -softening, $C_hD_h$ –hardening and the softening that proceeds beyond $D_h$. Correspondingly, there are a series of local modulus softening-hardening stages, which occur during cooling. In addition, the internal friction peak observed on heating has a corresponding tan δ maximum occurring on the cooling portion. All these features prove that the phenomena are reversible, during heating and cooling (Zhou, 2006). Considering: (i) the larger amount of thermally induced α'-bcc martensite, as compared to ε-hcp martensite, observed by XRD in 0_MA_700 specimens *(*Pricop *et al.*, 2014*)* and (ii) the association of the first internal friction peak, observed on heating, to the α'-bcc → γ-fcc and of the second to the ε-hcp → γ-fcc transformations, (Zhou, 2006), it can be assumed that the lower tan δ peak corresponds to the reversion of α'-bcc martensite to γ-fcc austenite and the higher one, located at larger temperatures, to the reversion of ε-hcp martensite. The former transformation started at $A_s^{\alpha'}$, reached the maximum at $A_{50}^{\alpha'}$ and ended at $A_f^{\alpha'}$. The latter transformation started at $A_s^{\varepsilon}$, which is approximately equal with $A_f^{\alpha'}$, reached the maximum at $A_{50}^{\varepsilon}$ and ended at $A_f^{\varepsilon}$, not represented in Fig. 2(b). The fact that tan δ did not reach the same value at the end of transformation, as before it, could be an effect of the 16.85 % porosity of 0_MA specimens. The critical temperatures $A_{50}^{\alpha'}$ and $A_{50}^{\varepsilon}$ were determined for all of the specimens, together with the increase in storage modulus, ΔE'. This modulus increase (hardening) and can be associated with the antiferromagnetic transition of γ-fcc austenite, occurring during heating at Néel temperature (Wu *et al.*, 2000), considering that a steep transition occurs, from antiferromagnetic to paramagnetic state, being accompanied by increases of storage modulus up to 15 GPa, within 50 K (Bouaziz *et al.*, 2011).

In order to emphasize the effects of heat treatment temperature on the damping behaviour of 0_MA specimens, cumulative diagrams are shown in Fig. 3.

The presence of modulus hardening, ΔE', in Fig. 3(a) and the two internal friction peaks of tan δ, in Fig. 3(b), are obvious on most of the diagrams. As mentioned, our attention will be focused on the storage modulus increasing step and on the first two internal friction peaks, observed during heating.

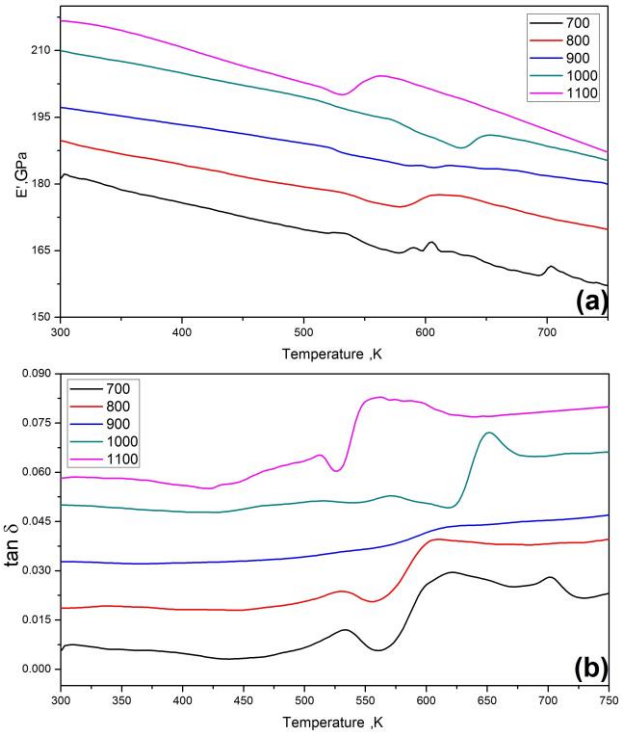


Fig. 3 Cumulative DMA thermograms illustrating the effects of heat treatment temperature (given in the inset, in $^0$C), on the behaviour of specimens 0_MA, during heating: (a) variation of storage modulus with temperature; (b) variation of internal friction with temperature.

It is noticeable that, at the specimens 0_MA_900, treated at 1173 K, martensite reversion to austenite is negligible. Both modulus hardening and internal friction peaks are the smoothest, as compared to the rest of the specimens. On the other hand, the behaviour of specimen 0_MA_1000, heat treated at 1273 K, represents an exception, since martensite reversion to austenite occurs at the most elevated temperatures. Disregarding these two thermograms, the other specimens experienced a tendency of $A_{50}^{\alpha'}$ and $A_{50}^{\varepsilon}$ to shift to lower values, with the increase of heat treatment temperature. Among these specimens, it is obvious that 0_MA_1100, heat treated at 1373 K, experienced the most marked increases of both E' and tan δ.

Aiming to further investigate the effects of MA fraction on the behaviour of the specimens solution treated at 1373 K, which caused the lowest transformation temperatures, the thermograms of the respective specimens were overlapped, as illustrated in Fig. 4.

Due to the large difference between the absolute values of E' and tan δ, characteristic to 20_MA_1100 specimens, as compared to the corresponding parameters observed at 10_MA_1100 specimens, the parameters of the latter reveal very small variations. It is obvious that 20_MA_1100 specimens have the steepest increases in storage modulus and the largest variations on internal friction.

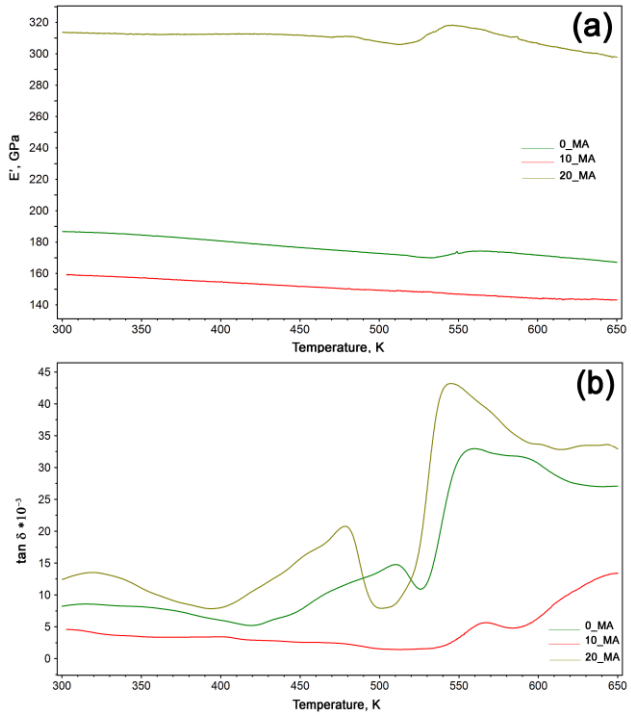


Fig. 4 DMA thermograms recorded on the specimens which were solution treated at 1373 K, illustrating the effects of MA fraction: (a) variation of storage modulus with temperature; (b) variation of internal friction with temperature

Thus, modulus hardening reached 6 GPa and tan δ first diminished with 0.013 at the end of α'-bcc → γ-fcc transformation, between $A_{50}^{\alpha'}$ and $A_f^{\alpha'}$ and then augmented with 0.035, at the beginning of ε-hcp → γ-fcc transformation, between $A_s^{\varepsilon}$ and $A_{50}^{\varepsilon}$, reaching the maximum internal friction value of 0.043.

A more general view of the effects of both solution treatment temperatures and MA fractions on the position of the two reverse martensitic transformations, $A_{50}^{\alpha'}$ and $A_{50}^{\varepsilon}$ and modulus hardening, ΔE', is offered by Fig. 5, which summaries the results obtained for 15 specimens.

From Figs. 5(a) and (b) it is obvious that the increase of MA fraction, to 20 vol. %, caused a marked tendency, of the two martensite reversions to austenite, to shift to lower temperatures. On the other hand, ΔE' reached the largest values at specimens 20_MA. In addition, the increase of heat treatment temperature, from 973, 1073 and finally to 1373 K was accompanied by general decreasing tendencies of $A_{50}^{\alpha'}$ and $A_{50}^{\varepsilon}$, for specimens 0_MA and 10_MA. For 20_MA a contrary tendency was noticed.

### 3.2 DMA during isothermal strain sweeps

During strain sweeps, besides tan δ, the variation of dynamic force ($F_{dyn}$) was also measured, which represents the maximum load applied by the pushrod. Strain sweeps were done at three different temperatures: (i) $T_1$ = RT, (ii) $A_s^{\varepsilon} < T_2 < A_{50}^{\varepsilon}$ and (iii) $T_3 > A_{50}^{\varepsilon}$, where internal friction was of interphase-boundary type but had two different causes.

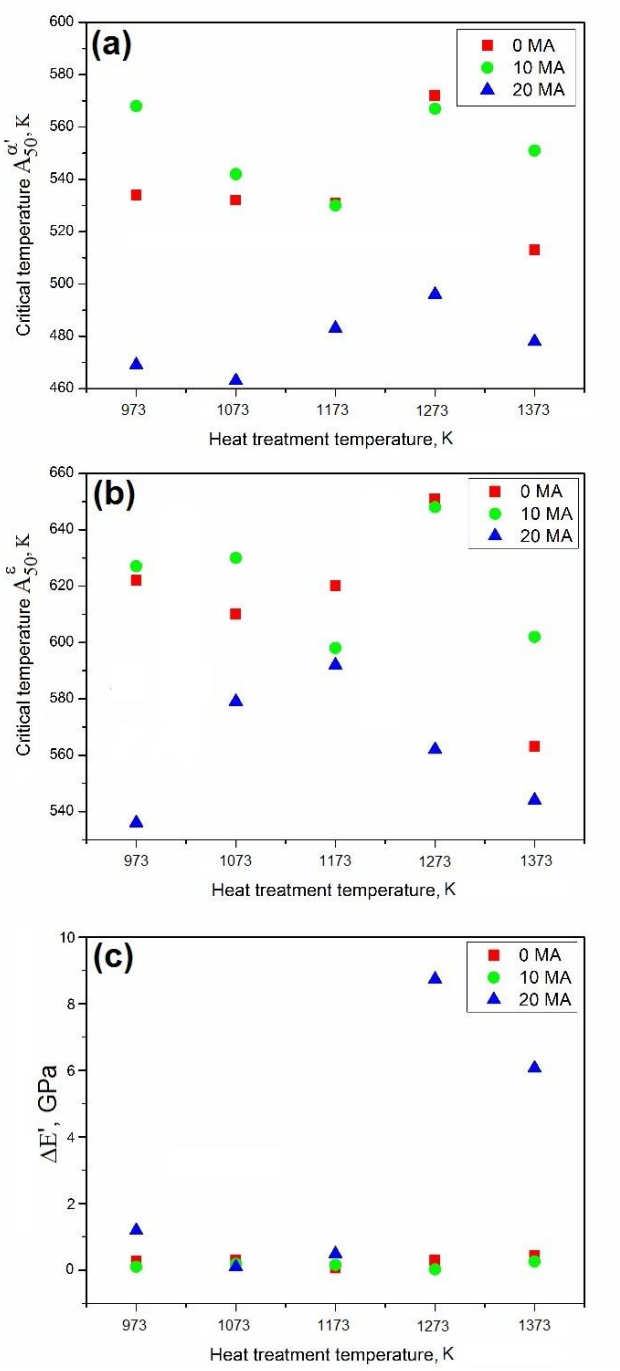


Fig. 5 Summary of the effects of solution treatment temperatures and MA fraction on the variation of characteristic parameters of DMA thermograms: (a) $A_{50}^{\alpha'}$; (b) $A_{50}^{\varepsilon}$ and (c) ΔE'

The former, occurring at $T_1$ = RT, consisted in the movement of interfaces while the latter, occurring at $T_2$ and $T_3$, results either from the movement of ε-hcp/ γ-fcc multiple interfaces or from the crystalline reorientations of ε-hcp/ γ-fcc phases.

During each of the three strain sweep bending cycles, tan δ and $F_{dyn}$ had different variations with strain amplitude, as exemplified in Fig.6, for the specimen 20_MA_1100, tested at the temperature $T_2$ = 533 K.

In the first cycle (solid line), $F_{dyn}$ had lower values that increased and stabilized in subsequent cycles,

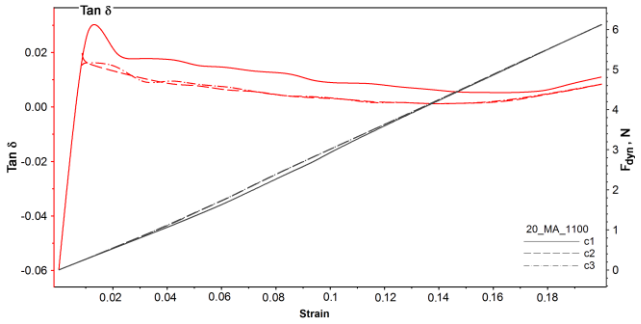


Fig. 6 Isothermal variations at $T_2$ = 533 K of internal friction (tan δ) and dynamic force ($F_{dyn}$) of specimen 20_MA_1100, as a function of amplitude

suggesting that the specimen was work hardened by dynamical loading. Concomitantly, tan δ experienced a large increase, at the beginning of the first cycle and became "smoother" in the subsequent ones. Due to PROTEUS software limitation, $F_{dyn}$ never exceeded a static threshold of 12 N, corresponding to a dynamic force of 8 N, which limited strain amplitude to 0.1.

In order to reveal the effects of solution treatment temperatures and MA fractions, logarithmic coordinates were used for both tan δ and $F_{dyn}$. In the following, the effects of: (i) strain sweep temperature, (ii) heat treatment temperature and (iii) MA fraction will be analysed based on the variations of average logarithmic tan δ and Fdyn with isothermal bending amplitude.

*The effects of strain sweep temperature* are exemplified by tan δ and $F_{dyn}$ variations, shown in Fig. 7, for three specimens 0_MA_700.

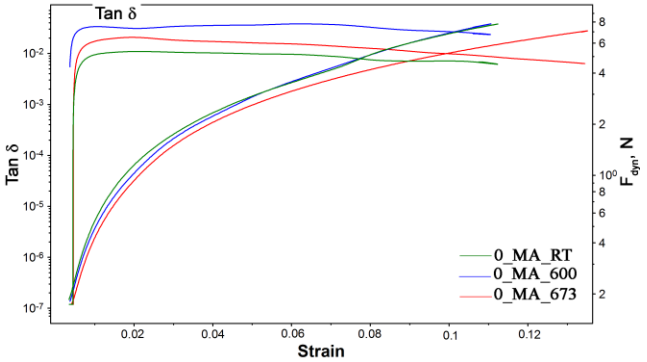


Fig. 7 Isothermal variations of average values of internal friction (tan δ) and dynamic force ($F_{dyn}$) of specimen 0_MA_700

It appears that, the strain sweep performed at RT = $T_1$ gave the lowest values of tan δ and the largest of $F_{dyn}$, within the strain amplitude range below 0.055. The lowest values of tan δ and the largest of $F_{dyn}$ were obtained at 11 and 7 specimens, respectively, tested at RT = $T_1$. On the other hand, the strain sweeps performed at the temperature $T_2$ gave the largest tan δ values and the same was noticed for 9 of the 15 variations under study.

So, it appears that tan δ variations with amplitude had the tendency to develop the lowest values due to the movement of the interfaces accompanying stress induced formation of martensite and the highest ones due to the reversible movement of the multiple martensite/ austenite interfaces and crystalline reorientations.

*The effects of heat treatment temperature* on isothermal logarithmic variation of internal friction are exemplified in Fig. 8 which illustrates average tan δ *vs.* strain amplitude for specimens 10_MA tested at temperature $T_2$ ($A_s^{\varepsilon} < T_2 < A_{50}^{\varepsilon}$).

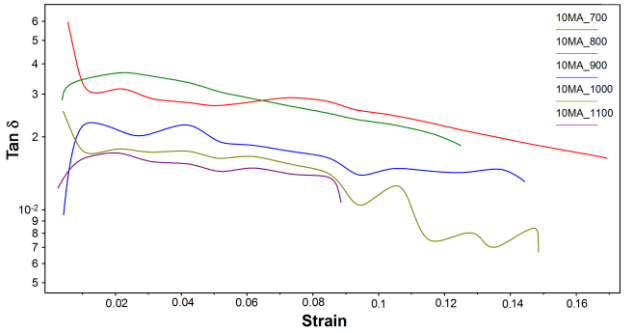


Fig. 8 Isothermal variations, at temperature $T_2$ ($A_s^{\varepsilon} < T_2 < A_{50}^{\varepsilon}$), of the average values of internal friction (tan δ) of specimen 10_MA

On most of the strain range, the average tan δ decreased with increasing heat treatment temperature. It appears that the solution treated specimens at 1173 K have the tendency to experience the lowest tan δ, which could be related to the lowest internal friction values, observed in Fig. 3, for these specimens.

*The effects of MA fraction* are less obvious than those of heat treatment temperature because the variation curves of tan δ, for different MA fraction, intersect each other, during amplitude variation. One typical variation is shown in Fig. 9, for specimens heat treated at 973 K, when tested at temperature $T_2$ where the largest internal friction values were observed.

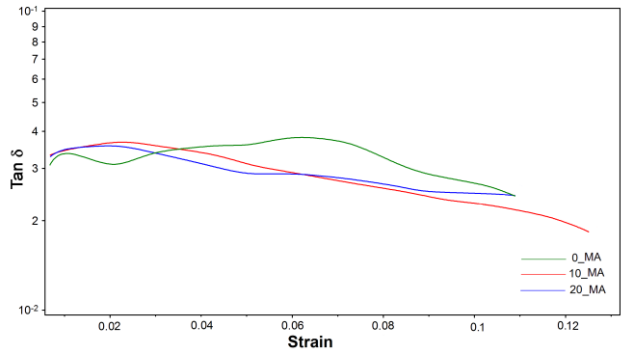


Fig. 9 Isothermal variations of average values of internal friction of the specimens heat treated at 937 K and tested at the temperature $T_2$, illustrating the effects of MA fraction.

It appears that mechanical alloying caused a rather uniform decreasing tendency of internal friction while simple powder-blending enabled periodic variations of tan δ, between 0.3 and 0.4, in the strain amplitude range below 0.09.

### 3.3 Structural analysis

The XRD patterns of Fig.10 summarize the influence of MA fraction on the specimens treated at 1373 K.

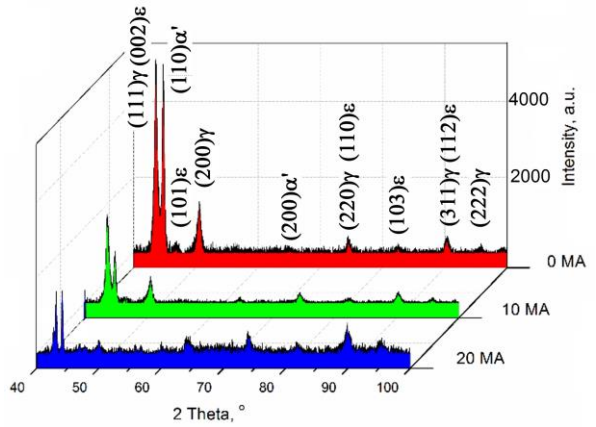


Fig. 10 Characteristic XRD patterns of the specimens heat treated at 1373 K

The amount of thermally induced α'-bcc martensite, had an increasing tendency from almost 46 % at 0_MA to approx. 50 % at 20_MA, while ε-hcp martensite experienced an increasing tendency from 19 to 23 %. Quantitative evaluations were performed with respect to the non-overlapping XRD maxima, namely: α'(110), ε(101), γ(200), α'(200), ε(103), γ(222).

It appears that the presence of thermally induced α'-bcc martensite could be the cause of the reduced value of internal friction, both during heating, see Figs. 2 and 3 and during isothermal strain sweep performed at RT, where the largest amounts of α' can be found.

## 4. CONCLUSIONS

From the point of view of the transitory term, $Q^{-1}_{Tr}$, which characterizes internal friction produced only during heating, the following variation tendencies were noticed:

- the transformation temperatures $A_{50}{}^{\alpha'}$ and $A_{50}{}^{\varepsilon}$, characteristic to the reversion to austenite of α'-bcc and ε-hcp martensites decreased with the increase of heat treatment temperature at the specimens heat treated at 973, 1073 and 1373 K;
- the specimens with largest MA fraction (20 vol. %) heat treated at the highest temperature, 1373 K, experienced the largest variation of storage modulus and internal friction;
- the increase of MA fraction to 20 vol. % caused a shift of $A_{50}{}^{\alpha'}$ and $A_{50}{}^{\varepsilon}$ to lower values.

From the point of view of the phase transition term, $Q_{-1}{}^{PT}$, which characterizes the internal friction only during isothermal strain sweep, being related to the reversible displacement of interfaces, the following variation tendencies were noticed:

- the lowest values of tan δ and the highest of $F_{dyn}$ were obtained at RT, where the largest amounts of α'-bcc existed;
- in the thermal range located in the first part of the ε-hcp → γ-fcc transformation, internal friction had the largest values.


### Acknowledgements

Dr. T. Sawaguchi, from NIMS Tsukuba and Assist. Prof. M. Koyama, from Kyushu University, are gratefully acknowledged for the fruitful discussions. This work was supported by UEFISCDI through project code PN.II-PT-PCCA-2011-3.1-0174, contract 144/ 2012.


### References


1. Baik, S. B. *et al.*, (1995), *Effects of carbon content and cold working on damping capacity and mechanical property of Fe-17 wt. % Mn martensitic alloy*, J. Phys. IV France, C8-391-C8-396.
2. Baik, S. H. et al., (1997), *Effects of alloying elements on martensitic transformation behaviour and damping capacity in Fe-17Mn alloy*, J. Phys. IV France, pp. C5-453- C5-458.
3. Baik, S. H. et al. (2006), *High damping Fe-Mn martensitic alloys for engineering applications*, Mater. Sci. Eng. A, 438-440, pp. 1101-1105.
4. Banks H. T., Pinter, G. A., (2001), *Hysteretic dumping*, Encyclopaedia on vibration, Academic Press 2001, pp. 658-664.
5. Bidaux, J.-E., et al., (1989), *Study of HCP-FCC phase transition in Cobalt by acoustic measurements*, Acta Metall., 37(3), pp. 803-811.
6. Bouaziz, O. et al., (2011), *High manganese austenitic twinning induced plasticity steels: a review of the microstructure properties relationships*, Curr. Opin. Solid. St. M. 15, pp. 141-168.
7. Bujoreanu, L. G. *et al.*, (2009), *Factors influencing the reversion of stress-induced martensite to austenite in a Fe-Mn-Si-Cr-Ni shape memory alloy*, J. Mater. Eng. Perform., 18, pp. 500-505.
8. Choi, C. S. et al., (1992), *Damping capacities in Fe-X % Mn martensitic alloys*, Proc. ICOMAT, Monterey, pp. 509-514.
9. Chou, T. S. et al., (2000), *Characterization of internal friction of Fe-30Mn-6Si-5Cr*, Scripta Mater., 42, pp. 445-450.
10. De Jongue, W. et al. (1976), *Factors affecting the internal friction peak due to thermoelastic martensitic transformation*, Scripta Metal., 10, pp. 1125-1128.
11. De, A. K. et al., (2002), *Fcc-hcp Transformation-Related Internal Friction in Fe-Mn Alloys*, Z. Metallkd., 93, 228-235.
12. Gavriljuk, V. G. et al., (1998), *Influence of nitrogen on vibration damping and mechanical properties of Fe-Mn alloys*, Scripta Mater., 38, pp. 931-935.
13. Granato, A., Lucke, D., (1956), *Theory of Mechanical Damping Due to Dislocations*, J. Apply.

Phys., 27, pp. 583-592.
14. Jee, K. K. *et al.*, (1985), *Transformation behaviour and its effect on damping capacity in Fe-Mn based alloys*, J. Phys. IV France, C8-385-C8-390. Jee, K. K. *et al.*, (1994), *Damping capacity in Fe-27Mn-3.5Si Alloy*, ISIJ Inter., 34, pp. 912-916.
15. Jee, K. K. *et al.*, (1997), *Damping capacity in Fe-Mn based alloys*, Scripta Mater., 37(7), pp. 943-948.
16. Kajiwara, S. (1999), *Characteristic features of shape memory effect and related transformation behaviour in Fe-based alloys*, Mater. Sci. Eng. A 1999, 273-275, pp. 67-88.
17. Kajiwara, S. *et al.*, (2001), *Development of Fe-Mn-Si based shape memory with no necessity of "training"*, J. Phys.V France, 11, Pr8-199-Pr8-204.
18. Kothalkar, A. *et al.*, (2014), *Thermo-mechanical Response and Damping Behaviour of Shape Memory Alloy–MAX Phase Composites*, Metall. Mater. Trans. A, 45A, pp. 2646-2658.
19. Lee, Y.-K. *et al.*, (1997), *Damping capacity of Fe-Mn binary alloys*, ISIJ Inter., 37(10), 1023-1030.
20. Lohan, N. M. *et al.*, (2011), *Heating rate effects on reverse martensitic transformation in a Cu–Zn–Al shape memory alloy*, Int. J. Mater. Res., 102, pp. 1345-1351.
21. Magalas, L. B. (2003), *Mechanical Spectroscopy – Fundamentals*, Solid State Phenom. 2003, 89, 1-22.
22. Min, X. H. *et al.*, (2013), *An attempt to lower Mn content of Fe–17Mn–6Si–0.3C shape memory alloy*, J. Alloy Compd., 577S, pp. S478-S-482.
23. Montecinos, S., (2015), *Influence of microstructural parameters on damping capacity in CuAlBe shape memory alloys*, Mater. Design, 68, 215-220.
24. Perez-Saez, R. B., *et al.* (1998), *Anelastic contributions and transformed volume fraction during thermoelastic martensitic transformations*, Phys. Rev. B, 57, pp. 5684-5692.
25. Pricop, B. *et al.*, (2012), *Thermal behaviour of mechanically alloyed powders used for producing an Fe-Mn-Si-Cr-Ni shape memory alloy*, J. Mater. Eng. Perform., 21, pp. 2407-2416.
26. Pricop, B. *et al.*, (2014), *Influence of mechanically alloyed fraction and hot rolling temperature in the last pass on the structure of Fe-14Mn-6Si-9Cr-5Ni (mass. %) shape memory alloys processed by powder metallurgy*, Optoelectron. Adv. Mat., 8, pp. 247-250.
27. Sato, A. *et al.*, (1988), *Internal friction due to $\varepsilon \rightarrow \gamma$ reverse transformation in an Fe-Mn-Si-Cr shape memory alloy*, Mater. Sci. Eng. A, 101, 25-30.
28. Sawaguchi, T. *et al.*, (2006a), *Vibration mitigation by reversible fcc/ hcp martensitic transformation during cyclic tension-compression loading of an Fe-Mn-Si-based shape memory alloy*, Scripta Mater., 54, pp. 1885-1890.
29. Sawaguchi, T. *et al.*, (2006b), *Internal friction of an Fe-28 Mn-6 Si-5 Cr-0.5 NbC shape memory alloy*, Mater. Sci. Eng. A, 438-440, pp. 796-799.
30. Sawaguchi, T. *et al.*, (2006c), *Internal friction of Fe-Mn-Si-based shape memory alloys containing Nb and C and their application as a seismic damping materials*, Key Eng. Mater., 319, pp. 53-58.
31. Sawaguchi, T. *et al.*, (2007), *Absorption of Seismic Vibration by Fe-Mn-Si-Based Shape Memory Alloys and TRIP/TWIP Steel*, Proc. SMST 2007, Tsukuba, pp. 637-644.
32. Sawaguchi, T. *et al.*, (2008), *Effects of Nb and C in solution and in NbC form on the transformation-related internal friction of Fe-17Mn (mass%) alloys*, ISIJ Int., 48, pp. 99-106.
33. Söyler, A. U. et al., (2010), *Sintering Densification and Microstructural Characterization of Mechanical Alloyed Fe-Mn-Si based Powder Metal System*, Suppl. Proc: Vol. 3 TMS, pp. 785-792.
34. Söyler, A. U. *et al.*, (2011), *Investigation of Mechanical Alloying Process Parameters on Fe-Mn-Si Based System*, Suppl. Proc.: Vol. 1: TMS, 577-583.
35. Söyler, A. U. *et al.*, (2014), *Improvement of shape memory characteristics of Fe-14Mn-6Si-9Cr-5Ni powder metallurgy alloy via mechanical alloying*, J. Mater. Eng. Perform., 23, pp. 2357-2361.
36. Spiridon, I. P. *et al.*, (2013), *The influence of heat treatment atmosphere and maintaining period on the homogeneity degree of a Fe-Mn-Si-Cr-Ni shape memory alloy obtained through powder metallurgy*, J Optoelectron. Adv. M., 15, pp. 730-733.
37. Stoiber, J., *et al.*, (1994), *The movement of single $\beta_1 \rightarrow \beta_1'$ interfaces in Cu-Zn-Al as studied by a new technique of internal friction measurement*, Acta Metal. Mater., 42, pp. 4059-4070.
38. Van Humbeeck, J. *et al.*, (1995), *The high damping capacity of shape memory alloys*, Z. Metallkd., 86, pp. 176-183.
39. Van Humbeeck, J., (2001), *The martensitic transformation*, Mater. Sci. Forum 366-368, 382-415.
40. Wan, J. *et al.*, (2006), *Modulus Softening during the c fi e Martensitic Transformation in Fe-25 Mn-6 Si-5 Cr-0.14 N Alloy*, Mat. Sci. Eng. A, 438-440, 887-890.
41. Wang, Q. Z. *et al.*, (2014), *Effects of aging on the structure and damping behaviours of a novel porous CuAlMn shape memory alloy fabricated by sintering–dissolution method*, Mat. Sci. Eng. A, 615, 278-282.
42. Wu, X. *et al.*, (2000), *Effect of the Neel temperature, $T_N$, on martensitic transformation in Fe–Mn–Si-based shape memory alloys*, Mater. Char., 45, pp. 137-142.
43. Zhou, Z. C. (2006), *Internal friction observation of the $\varepsilon \leftrightarrow \gamma$ transformation in a Fe–Mn alloy*, Mat. Sci. Eng. A, 438-440, pp. 336-338.

Received: November 5, 2015 / Accepted: June 10, 2016 / Paper available online: June 20, 2016 